Nano Research 2014, 7(11): 1680–1690
DOI 10.1007/s12274-014-0528-6
Research Article
ISSN 1998-0124
CN 11-5974/O4

Highly stretchable pseudocapacitors based on buckled reticulate hybrid electrodes

Nan Zhang[1,2], Pingshan Luan[1,2], Weiya Zhou[1] (✉), Qiang Zhang[1,2], Le Cai[1,2], Xiao Zhang[1,2], Wenbin Zhou[1,2], Qingxia Fan[1,2], Feng Yang[1,2], Duan Zhao[1,2], Yanchun Wang[1], and Sishen Xie[1] (✉)

[1] *Beijing National Laboratory for Condensed Matter Physics, Institute of Physics, Chinese Academy of Sciences, Beijing 100190, China*
[2] *University of Chinese Academy of Sciences, Beijing 100049, China*

Received: 14 May 2014
Revised: 20 June 2014
Accepted: 27 June 2014

KEYWORDS
single-walled carbon nanotubes,
supercapacitor,
stretchability,
all-solid-state,
nanocomposites,
polyaniline

ABSTRACT

In order to develop an excellent pseudocapacitor with both high specific capacitance and outstanding stretchability to match with other devices applicable in future wearable and bio-implantable systems, we focus our studies on three vital aspects: Stretchability of hybrid film electrodes, the interface between different components, and the integrated performance in stretchability and electrochemistry of supercapacitors based on single-walled carbon nanotube/polyaniline (SWCNT/PANI) composite films on pre-elongated elastomers. Owing to the moderate porosity, the buckled hybrid film avoids the cracking which occurs in conventional stretchable hybrid electrodes, and both a high specific capacitance of 435 $F \cdot g^{-1}$ and a high strain tolerance of 140% have been achieved. The good SWCNT/PANI interfacial coupling and the reinforced solid electrolyte penetration structure enable the integrated pseudocapacitors to have stretch-resistant interfaces between different units and maintain a high performance under a stretching of 120% elongation, even after 1,000 cyclic elongations.

1 Introduction

In order to meet the growing needs for portable electronics applicable in future wearable and bio-implantable systems, stretchable electronics, wherein circuits can be built- or embedded-in stretchable substrates, is emerging [1–5]. A variety of stretchable devices based on new structures and materials, such as stretchable conductors [6–10], light-emitting diodes (LED) [11], and other similar functional devices [12–19], have been investigated. To power these functional devices in a fully stretchable system, stretchability-matched and high performance energy storage devices are urgently needed. Owing to their high power density and cycling efficiency, some novel super-capacitors based on carbon materials have been fabricated [20–25]. Stretchable supercapacitors [26–31] have also gained a great deal of attention as stretchable

Address correspondence to Weiya Zhou, wyzhou@iphy.ac.cn; Sishen Xie, ssxie@iphy.ac.cn

power supply devices [32–36]. By adopting a pre-elongation strategy on an elastomer like polydimethylsiloxane (PDMS), several electric double layer capacitors (EDLC) with high stretchability have been designed [26–29]. Recently, in order to improve the specific capacitance of EDLC, pseudocapacitance has been introduced in stretchable energy storage devices by depositing pseudocapacitive materials on buckled Au film [30, 37] or on fabric [38]. However, restricted by the stretchability of hybrid pseudocapacitive materials and the configuration of the device, the stretchability of the buckled electrodes dramatically reduces after fabrication, and the limited elongation (about 30% elongation) or the poor elasticity of the existing device does not match with the fully stretchable integrated devices which require over 100% elongation [16, 17, 32]. Therefore, it is challenging to develop an excellent supercapacitor with both high stretchability and good electrochemical properties.

Essentially, three main issues play the vital roles in determining the properties of these supercapacitors and are our main focus of concern. The first is how to fabricate a hybrid electrode with high stretchability of over 100%. According to previous reports, cracks are common on the surface of hybrid buckled electrodes for stretchable devices, and hybrid films tend to form an irregular and large wavelength buckled structure, which has a negative influence on stretchability [30, 37, 39]. The second is how to maintain the good electrochemical performance of electrodes with highly stretchable structure. The third is how to achieve an interface with a strong coupling between different components. The strain tolerance of the interface is crucial, particularly for a stretchable device with much more complex interfacial structures, and is one of the key factors affecting the stability and durability of a supercapacitor.

In this paper, we report a highly stretchable, integrated pseudocapacitor based on free-standing single-walled carbon nanotube/polyaniline (SWCNT/PANI) reticulate hybrid films. To address the issues mentioned above, certain strategies were adopted. First of all, we tuned the content of PANI to improve the specific capacitance while preserving a moderate porosity of the hybrid film, which is the key for good network deformation capacity and good electrochemical properties. Then, a high interfacial strength introduced at the collector/pseudocapacitive materials interface ensured the stretch-resistance of the hybrid structure during stretching [40–42]. Finally, we adopted an electrolyte penetration structure that allowed solid electrolyte to infiltrate through the reticulate hybrid architecture and be in contact with PDMS, so that a good coupling formed at the electrode/elastomer interface. Based on these strategies, we achieved buckled SWCNT/PANI hybrid electrodes with 140% elongation ability, which possessed both an excellent specific capacitance of 435 $F \cdot g^{-1}$ and a high strain-tolerance porous structure. Highly stretchable and integrated supercapacitors were assembled, which retained excellent performance under stretching as high as over 120% elongation and could work properly even after 1,000 cyclic elongations of 120%. This might expand the utilization of pseudocapacitive materials for energy storage in highly stretchable electronics system.

2 Experimental

2.1 Preparation of SWCNT/PANI hybrid films

Freestanding SWCNT film was prepared by the floating catalyst chemical vapor deposition (FCCVD) method. More details can be found in our previous reports [43]. For purification and modification, the SWCNT film was immersed in HNO_3 (15 $mol \cdot L^{-1}$) for 4 h to remove the impurities and increase the number of hydrophilic functional groups (e.g., O=C–OH). Hydrophilic films favour the *in situ* polymerization process in aqueous solution [44, 45]. The electrolyte for electrodeposition consisted of 0.5 M H_2SO_4, 0.5 M Na_2SO_4 and 0.05 M aniline in aqueous solution [46]. Electrodeposition of PANI was performed in a traditional three-electrode cell (a saturated calomel electrode was used as reference electrode), as shown in Fig. S1(a) in the Electronic Supplementary Material (ESM). PANI was electrodeposited under a constant voltage of 0.75 V at room temperature. All chemicals were analytical grade and aniline was purified by distillation.

2.2 Preparation of PDMS substrate

Silicone elastomer (Sylgard 184, Dow Corning) was mixed with cross linker (10:1 by weight), and poured into a mould. After degassing in a vacuum chamber, the mixture was solidified at 70 ℃ for 0.5–1 h. The thickness of PDMS substrate can be controlled by adjusting the amount of silicone elastomer base and the area of the mould.

2.3 Preparation of buckled SWCNT/PANI hybrid films on PDMS

A schematic of the preparation of a buckled SWCNT/PANI hybrid film on a PDMS substrate is shown in Fig. S1(c) (in the ESM). Silicon PDMS of the desired size (5 cm × 3 cm × 0.05 cm) was fixed on the strain frame and stretched to 100% pre-elongation. Then, the freestanding hybrid film was spread out onto the pre-elongated PDMS substrate directly, and ethanol was dripped onto the surface of the SWCNT/PANI hybrid film to ensure flat and firm adhesion between SWCNT/PANI film and PDMS. Finally, the pre-elongated PDMS was released to the original length and a buckled hybrid film was formed on the PDMS substrate. It is important to note that several hybrid films can be spread onto the large substrate end to end by this method, which will scale up the area of SWCNT electrodes and resolve the limitation of SWCNT film area for large-scale supercapacitor electrodes.

2.4 Assembly of the integrated supercapacitors

Three grams of poly(vinyl alcohol) (PVA) and two grams of H_3PO_4 were added into 30 mL of water, and the solution was heated to 85 ℃ and stirred at this temperature for 2 h. Before assembling, metal leads were connected to the films. The hot solid electrolyte solution (H_3PO_4–PVA aqueous solution) was dripped onto the SWCNT/PANI films and coated over the whole electrode by a spin coater. After drying for 2 h, two hybrid electrodes with electrolyte gel were pressed together and dried for 12 h in a fume hood to complete the assembly.

2.5 Characterization and measurement

The morphology and the microstructures of SWCNT/PANI hybrid film were characterized by scanning electron microscopy (SEM, Hitachi S-4800) and transmission electron microscopy (TEM, Tecnai F20). The resistances of the films were measured by a Keithley 2400 digital SourceMeter. The mechanical properties were characterized by a dynamic mechanical analyzer (TA GG92-DMA Q800). The apparatus for the stretching operation was fixed at 1 cm, and the tensile rate was 1% per min. The thickness of the films was measured by a stylus profiler (Dektak 8). Cyclic voltammetry curves and charge/discharge curves were recorded by an electrochemical workstation (CHI 660C). The specific capacitance was calculated from the charge/discharge curves by using the equation $Cs = I \times \Delta t/(\Delta V \times m)$, where I is the applied current, Δt is the time of discharge, ΔV is the window potential, and m is the total mass of the two SWCNT/PANI hybrid film electrodes. The mass of a hybrid film was measured directly by a high precision balance (METTLER TOLEDO UMX2, the readability is 0.1 μg, and the repeatability (standard deviation) is 0.25 μg). The Raman spectra were obtained using a confocal microscopic optical system (LabRAM HR800, HORIBA Jobin Yvon Inc.).

3 Results and discussion

The free-standing porous SWCNT films with a thickness of about 200 nm, as shown in Fig. S2 (in the ESM), were prepared directly by an improved FCCVD technique [43]. The continuous reticulate architecture endows such films with superior electrical conductivity (about 2,000 $S \cdot cm^{-1}$) and higher strain tolerance than those of post-deposited SWCNT films. Thus, the as-synthesized SWCNT films have enormous potential for applications in composites and electrodes [43, 47]. The SWCNT/PANI hybrid film was synthesized by an *in situ* electrochemical polymerization technique. Figure S1(b) (in the ESM) is the optical image of a SWCNT/PANI hybrid film with a thickness of about 240 nm. However, these hybrid films cannot directly meet the demand of highly stretchable electrodes (> 100% elongation). Some novel strategies are required to deal with the tough issues mentioned in the introduction section.

To analyze the impact of the electrodeposition time on the stretchability, tensile tests on the free-standing SWCNT/PANI hybrid films were performed. Figure 1(a)

presents the strain–stress curves of the hybrid films at different electrodeposition times. With the increase of electrodeposition time, the Young's modulus (the slope of the curves) increased but the breaking elongation gradually decreased. It is shown that the stretchability of the SWCNT films deteriorated significantly after forming a composite with PANI, even down to half of the original strain tolerance after electrodeposition for only 15 s. The results reveal that the hybrid films are less suitable for direct use as stretchable electrodes than the original SWCNT films. However, for the SWCNT/PANI hybrid films, a moderate *in situ* polymerization of PANI is imperative for their high specific capacitance and energy density.

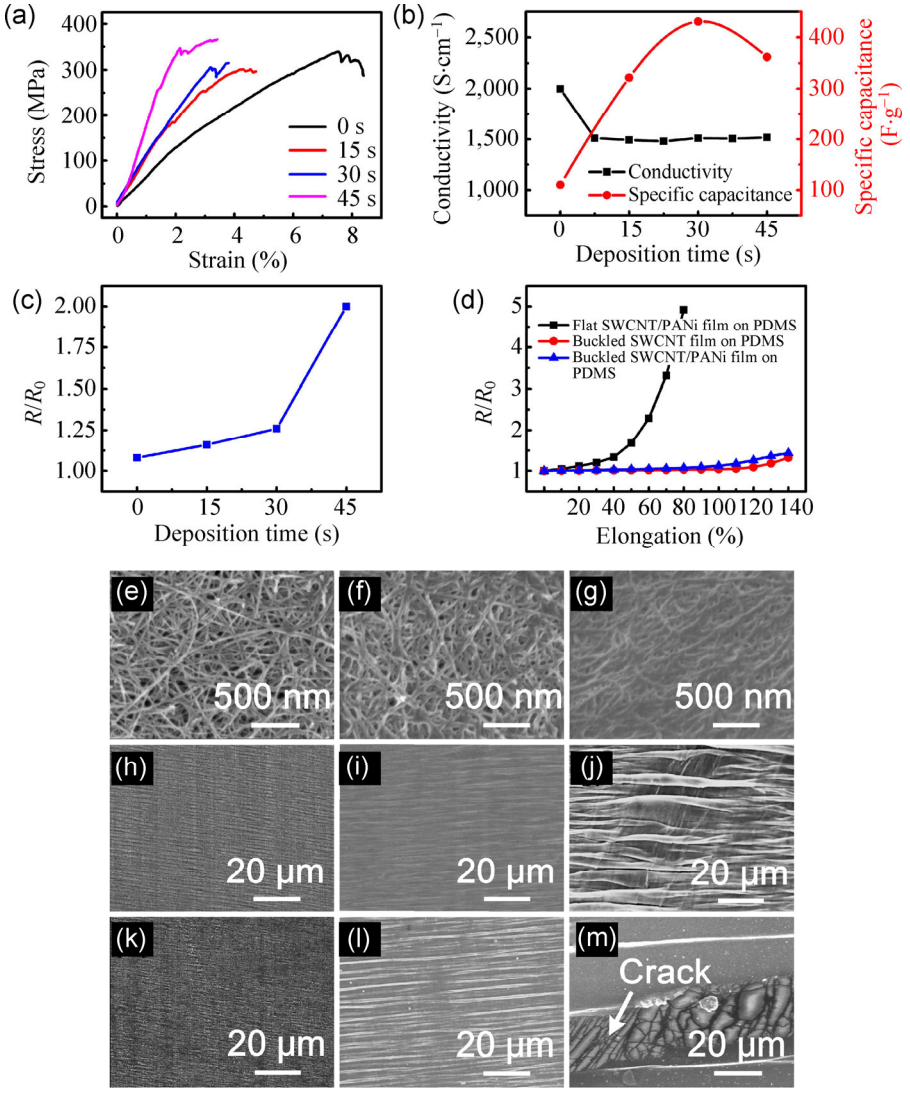

Figure 1 (a) Strain–stress curves of the SWCNT/PANI hybrid films at different electrodeposition times (0, 15, 30, and 45 s). (b) The conductivity (black squares) and the specific capacitance (red dots) of the hybrid films at different electrodeposition times (0, 15, 30, and 45 s). (c) The normalized resistance of the buckled SWCNT/PANI hybrid films at different electrodeposition times, where R_0 is the resistance of the unstretched hybrid films and R is the resistance of the hybrid films under 120% elongation. (d) The normalized resistance of SWCNT/PANI films (with 30 s polymerization of PANI) on PDMS with (black squares) and without (blue triangles) a buckled structure at different elongation levels, together with a comparative curve of a buckled SWCNT film on PDMS (red dots). SEM images of SWCNT/PANI films at different electrodeposition times: (e) 15 s, (f) 30 s, (g) 45 s. SEM images of buckled structures at different electrodeposition times before stretching: (h) 15 s, (i) 30 s, (j) 45 s, and after stretching to 120% elongation: (k) 15 s, (l) 30 s, (m) 45 s.

Therefore, it is vital to minimize the adverse effects of PANI in order to achieve both high stretchability and excellent electrochemical properties.

We measured the conductivity and specific capacitance of hybrid films formed with different electrodeposition times, as shown in Fig. 1(b). The conductivity decreased slightly in the early stage and then remained almost unchanged, which implies PANI does not severely affect the carrier transport in an electrode of a supercapacitor. This is probably because the highly conductive continuous SWCNT reticulations, which play a major role in conductivity [6], are preserved as a "skeleton" in the hybrid film, and the PANI acting as a "skin" merely affects the interbundle contacts [46]. This unique reticulate architecture has the advantage of transporting carriers and reacting with ions over a large area, ensuring a high power density of the supercapacitor while increasing capacitance. The specific capacitance of the hybrid film reached a maximum value of 435 $F \cdot g^{-1}$ at the deposition time of about 30 s, indicating that 30 s is the optimal electrodeposition time in terms of the electrochemical properties. Meanwhile, after introducing PDMS to provide pre-elongation and avoid stress concentration (see the scheme in Fig. S1(c)), the normalized resistance of the buckled electrodes under 120% elongation increased gradually below 30 s electrodeposition time and rapidly afterwards (Fig. 1(c)). Interestingly, this electrodeposition time coincides well with that for achieving maximum specific capacitance. This result reveals that the three vital factors (moderate porosity, ideal stretchability, good electrochemical properties) can be achieved simultaneously by optimizing control of the electrodeposition time. More importantly, Fig. 1(b) shows that the buckled hybrid film with the PANI electrodeposition time of 30 s maintained a superior conductivity of about 1,500 $S \cdot cm^{-1}$, which is still much higher than the stretchable conductive textile with SWCNT ink (125 $S \cdot cm^{-1}$) [48]. Thus, these results enable us to determine the optimal polymerization parameters for preparing the best buckled hybrid films with both high stretchability and excellent electrochemical properties for stretchable supercapacitor applications. To further reveal the performance of the optimal electrode, the dependence of its capacitance on the current density is presented in Fig. S3 (in the ESM).

In order to explore the maximum elongation of the optimal electrodes, the resistances of periodically buckled or flat films on PDMS under different strain levels were tested accordingly, as shown in Fig. 1(d). For the optimal hybrid film without a buckled structure, the resistance increased slightly with the strain below 40% elongation and rapidly beyond. Contrastingly, the resistance of the buckled optimal hybrid film was nearly unchanged up to 140% elongation and showed a similar behaviour to the buckled pure SWCNT film. It is absolutely vital to keep the resistance of electrodes unchanged under increasing strain, since the resistance of the hybrid film will affect the performance of stretchable supercapacitors.

Such an improvement in stretchability and high specific capacitance of the buckled optimal hybrid film can be ascribed to its unique microstructure. The deformation of the reticulate structure is the main way to endure strain beyond pre-elongation, and the high capacitance also relies on the diffusion of electrolyte in the pores. Therefore, retaining the moderate porosity is crucial to achieve superior performance in mechanics and electrochemistry. Figures 1(e)–1(g) show that the pores were filled gradually by PANI with increasing electrodeposition time. The optimal porous architecture was achieved in the hybrid film with an electrodeposition time of 30 s, while the other films incorporated insufficient PANI or involved many closed pores. The proper porosity of the film ensures both high specific capacitance and mesh deformation. Once the SWCNT network is filled by excessively deposited inelastic PANI, the hybrid film with closed pores cannot endure large elongation via a free deformation of reticulation. At the same time, its specific capacitance declines due to bad diffusion of the electrolyte.

In order to better illustrate the variation of the films after elongation, SEM images of the buckled structure before and after 120% stretching are presented in Figs. 1(h)–1(m). When the electrodeposition time was between 0 and 30 s, the small-wavelength buckled structure was regular before stretching (Figs. 1(h) and 1(i)). After stretching, the morphology of the

buckled structure was basically maintained and no obvious cracking was found on the surface of the hybrid film (Figs. 1(k) and 1(l)). However, when the electrodeposition time increased to 45 s, the buckled structure was irregular even before stretching (Fig. 1(j)). After stretching (Fig. 1(m)), it can be clearly observed that the buckled structure was damaged and large cracks appeared on the surface of the hybrid film. Therefore, under the optimal conditions (30 s electrodeposition time), the combination of the unique network deformation capacity and the buckled structure enables the buckled SWCNT/PANI hybrid films, with a small wavelength of 3 μm and a regular structure, to possess both high stretchability and good electrochemical properties. Though the reticulate hybrid films showed a relatively low breaking elongation (Fig. 1(a)), the optimal hybrid film on PDMS could still achieve a highly stretchability (140% elongation, Fig. 1(d)), fully meeting the demand of highly stretchable hybrid electrodes.

The process of assembling a supercapacitor is shown in Fig. 2(a). The H_3PO_4–PVA solid electrolyte and buckled SWCNT/PANI/PDMS electrodes were prepared first. Then, the solid electrolyte solution was dripped into the hybrid electrode and spread over the film by a spin coater. Finally, the H_3PO_4–PVA solid electrolyte layers on either electrode surface were face-to-face glued into one layer as a separator, forming the integrated stretchable supercapacitors (as shown in Fig. 2(b)), which could power a red LED, as shown in Figs. 2(c) and 2(d).

In this case, the H_3PO_4–PVA offers three functionalities: As electrolyte, separator and adhesive, leading to a simplified, reinforced and integrated configuration. In particular, the third function of the H_3PO_4–PVA gel tends to enhance the interfacial strength between the electrodes and PDMS. Figures 3(a)–3(c) illustrate a schematic view and SEM images of the interfacial structure in an integrated supercapacitor. The H_3PO_4–PVA solid electrolyte penetrated through the porous structure and acted as adhesive between hybrid electrode and PDMS. As shown in Fig. S4 (in

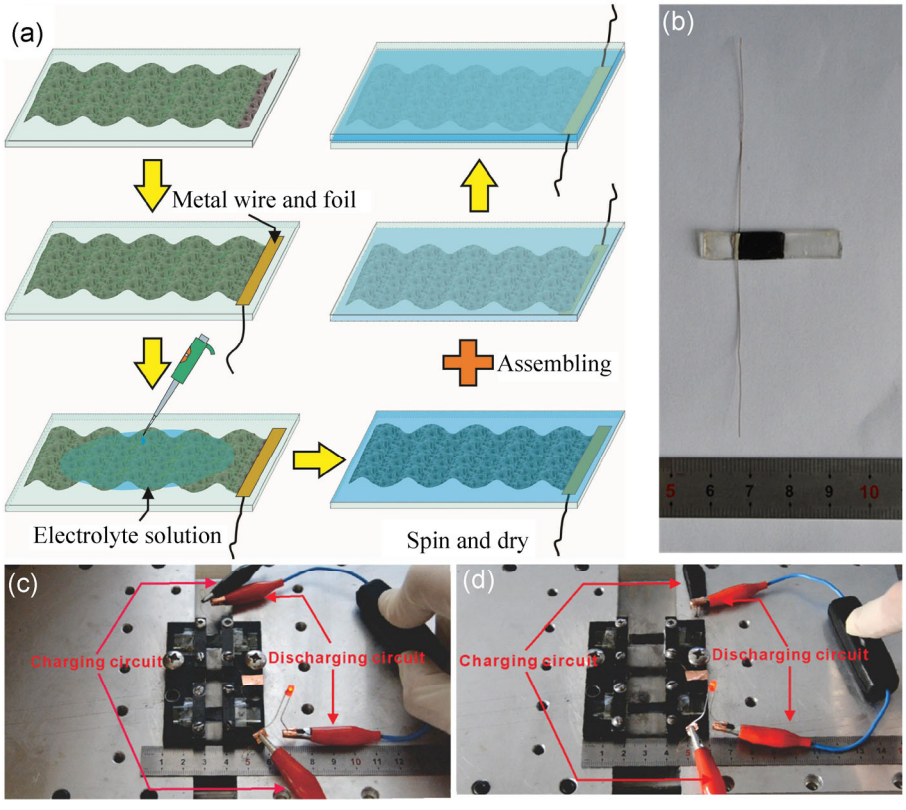

Figure 2 (a) Schematic of assembling the stretchable supercapacitor. (b) Optical image of the integrated stretchable supercapacitor. Optical image of integrated stretchable supercapacitors powering a red LED (c) without elongation and (d) with 120% elongation.

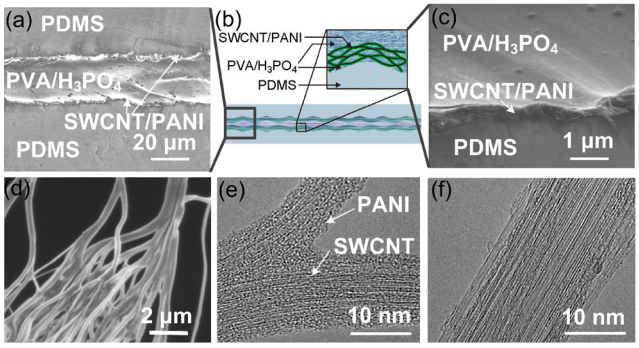

Figure 3 (a) SEM image of the integrated supercapacitor cross-section structure. (b) Schematic of the interfacial structure in the supercapacitor. (c) High magnification SEM image of the cross-section structure around the hybrid electrode in the supercapacitor. (d) SEM image of the SWCNT/PANI hybrid bundle in the fracture edge. (e) TEM image of SWCNT/PANI hybrid bundles after 50 cycles in 120% tensile elongations. The electrodeposition time of the hybrid film above was 30 s. (f) TEM image of a pure SWCNT bundle.

the ESM), for the buckled SWCNT/PANI films with PVA as an adhesive, the resistance was fairly stable during 1,000 cycles of elongation. However, the resistance of buckled SWCNT/PANI films without PVA varied slightly in the first cycle, but increased rapidly after several cyclic elongations. The increase in resistance may result from the separation between the electrode and PDMS during stretching, which might lead to damage of the hybrid film. The strong binding between the electrode and PDMS by interpenetrating PVA can promote a uniform strain transfer and avoid local stress concentrations [6], which enhances the stretchability of the hybrid films and improving the durability of the device. The results demonstrate that the structure of the as-integrated stretchable supercapacitor within PVA-reinforced interfaces is superior to that based on the non-porous metal electrodes or liquid electrolytes.

It is clear that the excellent and stable performance of the supercapacitor relies on the strong interfacial coupling between various components. Figure 3(b) shows that the configuration of the supercapacitor is PDMS/PVA/PANI/SWCNT//PVA//SWCNT/PANI/PVA/PDMS, including a series of interfaces, such as SWCNT/PANI, PVA/PANI, PDMS/PVA, or PDMS/PANI. All the interfacial couplings are between polymers and PVA or enhanced by PVA, except for SWCNT/PANI. Thus, it is critical to investigate the effect of stretching on the SWCNT/PANI interface. In Fig. 3(d), SEM images of the intentionally snapped hybrid film show that the PANI coated on the bundles could be deformed by the tensile stress along with SWCNT reticulation. Raman spectra, shown in Fig. S5 (in the ESM), indicate the formation of PANI on the SWCNT film. Moreover, in contrast to the TEM image of a pure SWCNT film (Fig. 3(f)), the nanoscale layer of PANI is clearly observed on the surface of the SWCNT after 50 stretch/release cycles in Fig. 3(e). No cracking and fragmentation is found on the surface of the SWCNT/PANI film. This demonstrates that the interface between SWCNT bundles and PANI can endure the stress during the stretching process. Two factors may be responsible for the good coupling between PANI and SWCNT even after stretching. Firstly, hydrophilic and clean SWCNT bundles pretreated by HNO_3 have a better contact with aqueous solution, which enables the aniline to polymerize on the surface of bundles directly during electrodeposition [41, 46]. Secondly, the interaction between SWCNT and PANI is believed to involve π–π stacking interactions [40–42], which results in a stable interfacial strength.

Cyclic voltammograms (CVs) are usually used to analyze the performance of a supercapacitor. In Fig. (a), the CVs of the as-integrated supercapacitor exhibit similar shapes within a selected range of potential from 5 $mV \cdot s^{-1}$ to 50 $mV \cdot s^{-1}$, indicating the stable and typical electrochemical performance of the SWCNT/PANI supercapacitor without elongation. The rectangular shape is evidence of a rapid current response on voltage reversal and the low equivalent series resistance (ESR) for the entire device. Additionally, from CV curves in Fig. S6 (in the ESM), it can be seen that the supercapacitor composed of the optimal films (30 s) achieved the highest specific capacitance. Calculated from the typical galvanostatic charge–discharge curves of the supercapacitor without elongation (Fig. 4(b)), the specific capacitance is 106 $F \cdot g^{-1}$ (at a current density of 1 $A \cdot g^{-1}$, the mass is the total mass of two hybrid films) which is better than that of the stretchable supercapacitors reported previously. In addition, the energy density is 8.3 $W \cdot h \cdot kg^{-1}$, and the power density is 20.1 $kW \cdot kg^{-1}$. The galvanostatic charge–discharge curves of the 1st, 100th, and 200th cycle are presented in Fig. S7 (in the ESM). The specific

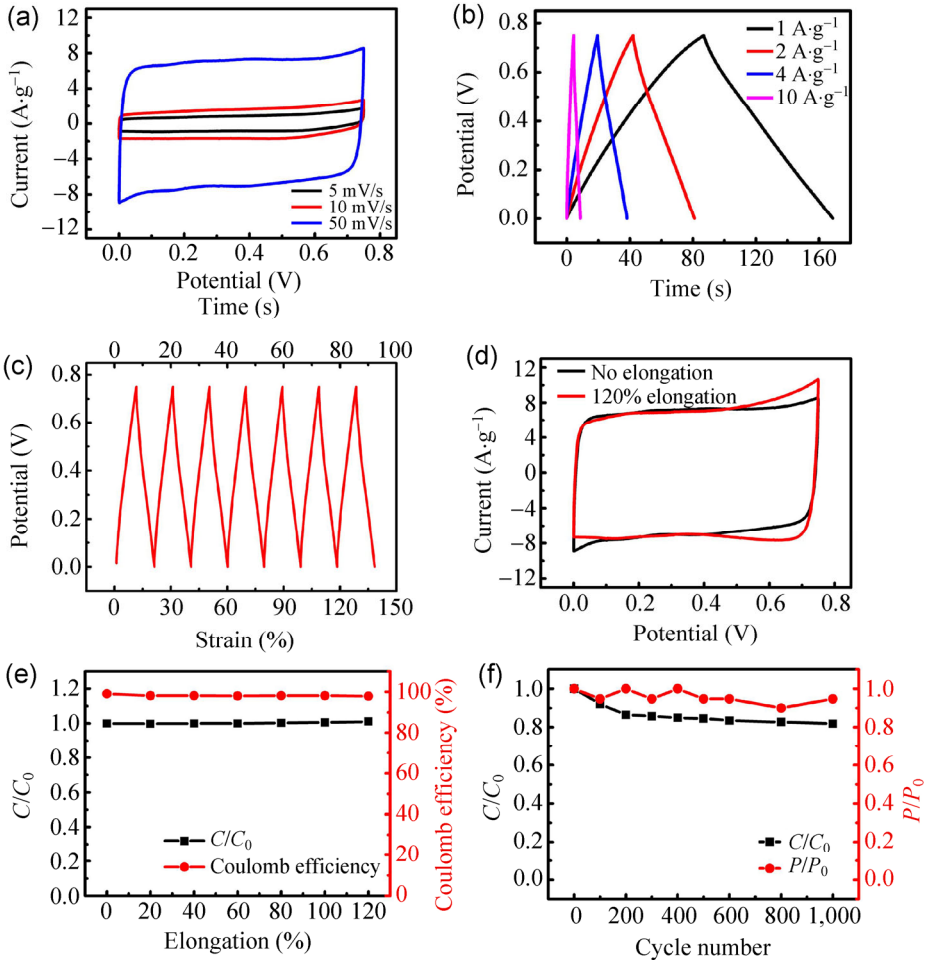

Figure 4 (a) CV curves of an integrated stretchable supercapacitor without elongation at different sweep rates (5 mV·s^{-1}, 10 mV·s^{-1}, and 50 mV·s^{-1}). (b) Charge and discharge curves of an integrated stretchable supercapacitor without elongation at different current densities (1 A·g^{-1}, 2 A·g^{-1}, 4 A·g^{-1}, and 10 A·g^{-1}), respectively. (c) Dynamic charge and discharge curves of an integrated supercapacitor at a constant current of 10 A·g^{-1} while the supercapacitor was stretched at a constant speed of 1.5% elongation per second. (d) CV curves of an integrated stretchable supercapacitor without elongation and with 120% elongation at a sweep rate of 50 mV·s^{-1}. (e) The variations of specific capacitance and coulomb efficiency at different elongation levels. (f) The variations of specific capacitance and power density after cyclic elongation of 120% at the tensile rate of 10% elongation per second, where C and P are the specific capacitance and power density after a certain number of stretching cycles, and C_0 and P_0 are the original specific capacitance and power density without any elongation, respectively.

capacitance maintained 86.3% of its original value after 100 cycles and then decreased to 82.6% at the 200th cycle, which confirms the electrochemical stability during cyclic charging and discharging.

A dynamic test was carried out to test the galvanic stability and the maximum elongation of the supercapacitor. Charge and discharge curves were tested with the supercapacitor being stretched at the rate of 1.5% elongation per second. Figure 4(c) shows that the supercapacitor can be stretched to over 120% elongation without any noticeable decay in capacitance, which is significantly better than the performance of other stretchable pseudocapacitors, and the similar shapes of different charge and discharge cycles indicate the galvanic stability under elongation. In Fig. 4(d), compared with the CV curve of the supercapacitor without elongation, the CV curve of the supercapacitor with 120% elongation at a sweep rate of 50 mV·s^{-1} has basically the same shape and area. Moreover, the capacitance and the coulomb efficiency of the integrated device are also nearly constant under different elongation level as shown in Fig. 4(e), indicating the

stability of the stretchable supercapacitor.

The supercapacitor also exhibits excellent stretchability and stability under repeated cyclic elongations. In Fig. 4(f), the black squares and red dots represent the variation of normalized specific capacitance (C/C_0) and power density (P/P_0) after 1,000 cyclic elongations of 120%, respectively. The specific capacitance retained 85% of its original value after 200 cycles and then remained nearly unchanged up to 1,000 cycles. The small decrease in power density implies that the supercapacitor has a high and stable power output even under a fatigue state, which is very important for the practical applications of a supercapacitor. The attenuation of performance might be due to an increase in resistance and damage of the reticulation in the preliminary stage of stretching. After the conditioning stage, which stabilizes the hybrid reticulate architecture, the specific capacitance and the power density gradually become stable. It is worth mentioning that the stretchable supercapacitor manifests a satisfactory electrochemical stability after storage for one month in air.

4 Conclusions

We have fabricated a highly stretchable and stable pseudocapacitor with excellent characteristics based on SWCNT/PANI reticulate hybrid films. Appropriate amounts of PANI were electrodeposited on the SWCNT continuous reticulation by *in situ* polymerization to improve specific capacitance and preserve the porosity. The introduction of a hybrid structure with optimized porosity avoids cracking during stretching and enables the buckled hybrid electrodes to possess high stretchability of 140% elongation and good specific capacitance of 435 $F \cdot g^{-1}$ (for a single electrode) simultaneously. Owing to the multi-functionality of PVA and the good interaction between conducting polymer and SWCNTs, the supercapacitor has not only an optimal configuration but also strong stretch-resistive interfaces between different components. Due to the adoption of these unique strategies, the integrated stretchable supercapacitor achieves improved specific capacitance of 106 $F \cdot g^{-1}$ and high stretchability of over 120%. It works well even after 1,000 cyclic elongations of 120%, which is significantly superior to the conventional stretchable supercapacitors fabricated using other materials and shows more promise for applications in highly stretchable energy storage devices. The stretchable and reticulate SWCNT/PANI nanocomposites can also be used in biomimetic and portable devices, such as cyber skin for robots and electrodes for wearable electronic systems. With the improvement in design and assembling techniques, high performance stretchable supercapacitors along with other stretchable functional devices should greatly change people's life-style in the future.

Acknowledgements

This work was supported by the National Basic Research Program of China (Grant No. 2012CB932302), the National Natural Science Foundation of China (Nos. 51172271, 51372269, and 90921012), the "Strategic Priority Research Program" of the Chinese Academy of Sciences (No. XDA09040202), and the Beijing Municipal Education Commission (Grant No. YB20108000101). We also thank Prof. Xiaoli Dong and Mr. Yue Wu for their assistance in measurement of the electrode mass.

Electronic Supplementary Material: Supplementary material (the schematics of preparing buckled SWCNT/PANI hybrid electrodes, the SEM images of a pure SWCNT film, the normalized capacitance of the optimal electrode at different current density, the resistance of buckled films during repeated elongations, the Raman spectra of SWCNT/PANI film, the CV curves of typical supercapacitors fabricated by different electrodes under 120% elongation and the charge/discharge curves at 1st, 100th, and 200th cycles) is available in the online version of this article at http://dx.doi.org/10.1007/s12274-014-0528-6.

References

[1] Khang, D. Y.; Rogers, J. A.; Lee, H. H. Mechanical buckling: Mechanics, metrology, and stretchable electronics. *Adv. Funct. Mater.* **2008**, *19*, 1526–1536.

[2] Kim, D. H.; Lu, N. S.; Ma, R.; Kim, Y. S.; Kim, R. H.; Wang, S. D.; Wu, J.; Won, S. M.; Tao, H.; Islam, A. et al. Epidermal electronics. *Science* **2011**, *333*, 838–843.

[3] Kim, D. H.; Rogers, J. A. Stretchable electronics: Materials strategies and devices. *Adv. Mater.* **2008**, *20*, 4887–4892.

[4] Maiti, U. N.; Lee, W. J.; Lee, J. M.; Oh, Y.; Kim, J. Y.; Kim, J. E.; Shim, J.; Han, T. H.; Kim, S. O. 25th anniversary article: Chemically modified/doped carbon nanotubes and graphene for optimized nanostructures and nanodevices. *Adv. Mater.* **2014**, *26*, 40–67.

[5] Rogers, J. A.; Someya, T.; Huang, Y. Materials and mechanics for stretchable electronics. *Science* **2010**, *327*, 1603–1607.

[6] Cai, L.; Li, J. Z.; Luan, P. S.; Dong, H. B.; Zhao, D.; Zhang, Q.; Zhang, X.; Tu, M.; Zeng, Q. S.; Zhou, W. Y. Highly transparent and conductive stretchable conductors based on hierarchical reticulate single-walled carbon nanotube architecture. *Adv. Funct. Mater.* **2012**, *22*, 5238–5244.

[7] Chun, K. Y.; Oh, Y.; Rho, J.; Ahn, J. H.; Kim, Y. J.; Choi, H. R.; Baik, S. Highly conductive, printable and stretchable composite films of carbon nanotubes and silver. *Nat. Nanotechnol.* **2010**, *5*, 853–857.

[8] Zhang, Y.; Sheehan, C. J.; Zhai, J.; Zou, G.; Luo, H.; Xiong, J.; Zhu, Y. T.; Jia, Q. X. Polymer-embedded carbon nanotube ribbons for stretchable conductors. *Adv. Mater.* **2010**, *22*, 3027–3031.

[9] Zhu, Y.; Xu, F. Buckling of aligned carbon nanotubes as stretchable conductors: A new manufacturing strategy. *Adv. Mater.* **2012**, *24*, 1073–1077.

[10] Zu, M.; Li, Q. W.; Wang, G. J.; Byun, J. H.; Chou, T. W. Carbon nanotube fiber based stretchable conductor. *Adv. Funct. Mater.* **2013**, *23*, 789–793.

[11] Sekitani, T.; Nakajima, H.; Maeda, H.; Fukushima, T.; Aida, T.; Hata, K.; Someya, T. Stretchable active-matrix organic light-emitting diode display using printable elastic conductors. *Nat. Mater.* **2009**, *8*, 494–499.

[12] Cai, L.; Song, L.; Luan, P.; Zhang, Q.; Zhang, N.; Gao, Q.; Zhao, D.; Zhang, X.; Tu, M.; Yang, F. et al. Super-stretchable, transparent carbon nanotube-based capacitive strain sensors for human motion detection. *Sci. Rep.* **2013**, *3*, 3038.

[13] Chen, Y.; Xu, Y.; Zhao, K.; Wan, X.; Deng, J.; Yan, W. Towards flexible all-carbon electronics: Flexible organic field-effect transistors and inverter circuits using solution-processed all-graphene source/drain/gate electrodes. *Nano Res.* **2010**, *3*, 714–721.

[14] Hu, X. L.; Krull, P.; de Graff, B.; Dowling, K.; Rogers, J. A.; Arora, W. J. Stretchable inorganic-semiconductor electronic systems. *Adv. Mater.* **2011**, *23*, 2933–2936.

[15] Khang, D. Y.; Jiang, H. Q.; Huang, Y.; Rogers, J. A. A stretchable form of single-crystal silicon for high-performance electronics on rubber substrates. *Science* **2006**, *311*, 208–212.

[16] Kim, D. H.; Song, J.; Choi, W. M.; Kim, H. S.; Kim, R. H.; Liu, Z.; Huang, Y. Y.; Hwang, K. C.; Zhang, Y. W.; Rogers, J. A. Materials and noncoplanar mesh designs for integrated circuits with linear elastic responses to extreme mechanical deformations. *Proc. Natl. Acad. Sci. USA* **2008**, *105*, 18675–18680.

[17] Kubo, M.; Li, X.; Kim, C.; Hashimoto, M.; Wiley, B. J.; Ham, D.; Whitesides, G. M. Stretchable microfluidic radiofrequency antennas. *Adv. Mater.* **2010**, *22*, 2749–2752.

[18] Yamada, T.; Hayamizu, Y.; Yamamoto, Y.; Yomogida, Y.; Izadi-Najafabadi, A.; Futaba, D. N.; Hata, K. A stretchable carbon nanotube strain sensor for human-motion detection. *Nat. Nanotechnol.* **2011**, *6*, 296–301.

[19] Yeo, W. H.; Kim, Y. S.; Lee, J.; Ameen, A.; Shi, L.; Li, M.; Wang, S.; Ma, R.; Jin, S. H.; Kang, Z. et al. Multifunctional epidermal electronics printed directly onto the skin. *Adv. Mater.* **2013**, *25*, 2773–2778.

[20] Niu, Z.; Chen, J.; Hng, H. H.; Ma, J.; Chen, X. A leavening strategy to prepare reduced graphene oxide foams. *Adv. Mater.* **2012**, *24*, 4144–4150.

[21] Niu, Z.; Liu, L.; Zhang, L.; Shao, Q.; Zhou, W.; Chen, X.; Xie, S. A universal strategy to prepare functional porous graphene hybrid architectures. *Adv. Mater.* **2014**, *26*, 3681–3687.

[22] Niu, Z.; Zhang, L.; Liu, L.; Zhu, B.; Dong, H.; Chen, X. All-solid-state flexible ultrathin micro-supercapacitors based on graphene. *Adv. Mater.* **2013**, *25*, 4035–4042.

[23] Niu, Z.; Zhou, W.; Chen, J.; Feng, G.; Li, H.; Ma, W.; Li, J.; Dong, H.; Ren, Y.; Zhao, D. et al. Compact-designed supercapacitors using free-standing single-walled carbon nanotube films. *Energy Environ. Sci.* **2011**, *4*, 1440–1446.

[24] Chen, P.; Chen, H.; Qiu, J.; Zhou, C. Inkjet printing of single-walled carbon nanotube/RuO_2 nanowire supercapacitors on cloth fabrics and flexible substrates. *Nano Res.* **2010**, *3*, 594–603.

[25] Meng, C. Z.; Liu, C. H.; Chen, L. Z.; Hu, C. H.; Fan, S. S. Highly flexible and all-solid-state paper like polymer supercapacitors. *Nano Lett.* **2010**, *10*, 4025–4031.

[26] Kim, D.; Shin, G.; Kang, Y. J.; Kim, W.; Ha, J. S. Fabrication of a stretchable solid-state micro-supercapacitor array. *ACS Nano* **2013**, *7*, 7975–7982.

[27] Li, X.; Gu, T. L.; Wei, B. Q. Dynamic and galvanic stability of stretchable supercapacitors. *Nano Lett.* **2012**, *12*, 6366–6371.

[28] Niu, Z. Q.; Dong, H. B.; Zhu, B. W.; Li, J. Z.; Hng, H. H.; Zhou, W. Y.; Chen, X. D.; Xie, S. S. Highly stretchable, integrated supercapacitors based on single-walled carbon nanotube films with continuous reticulate architecture. *Adv. Mater.* **2012**, *25*, 1058–1064.

[29] Yu, C. J.; Masarapu, C.; Rong, J. P.; Wei, B. Q.; Jiang, H. Q. Stretchable supercapacitors based on buckled single-walled

carbon nanotube macrofilms. *Adv. Mater.* **2009**, *21*, 4793–4797.

[30] Zhao, C.; Wang, C.; Yue, Z.; Shu, K.; Wallace, G. G. Intrinsically stretchable supercapacitors composed of polypyrrole electrodes and highly stretchable gel electrolyte. *ACS Appl. Mater. Inter.* **2013**, *5*, 9008–9014.

[31] Pasta, M.; La Mantia, F.; Hu, L.; Deshazer, H. D.; Cui, Y. Aqueous supercapacitors on conductive cotton. *Nano Res.* **2010**, *3*, 452–458.

[32] Gaikwad, A. M.; Zamarayeva, A. M.; Rousseau, J.; Chu, H. W.; Derin, I.; Steingart, D. A. Highly stretchable alkaline batteries based on an embedded conductive fabric. *Adv. Mater.* **2012**, *24*, 5071–5076.

[33] Kaltenbrunner, M.; Kettlgruber, G.; Siket, C.; Schwödiauer, R.; Bauer, S. Arrays of ultracompliant electrochemical dry gel cells for stretchable electronics. *Adv. Mater.* **2010**, *22*, 2065–2067.

[34] Lee, H.; Yoo, J. K.; Park, J. H.; Kim, J. H.; Kang, K.; Jung, Y. S. A stretchable polymer–carbon nanotube composite electrode for flexible lithium-ion batteries: Porosity engineering by controlled phase separation. *Adv. Energy Mater.* **2012**, *2*, 976–982.

[35] Lipomi, D. J.; Tee, B. C. K.; Vosgueritchian, M.; Bao, Z. N. Stretchable organic solar cells. *Adv. Mater.* **2011**, *23*, 1771–1775.

[36] Wang, Z. L. Energy harvesting for self-powered nanosystems. *Nano Res.* **2008**, *1*, 1–8.

[37] Wang, C. Y.; Zheng, W.; Yue, Z. L.; Too, C. O.; Wallace, G. G. Buckled, stretchable polypyrrole electrodes for battery applications. *Adv. Mater.* **2011**, *23*, 3580–3584.

[38] Yue, B. B.; Wang, C. Y.; Ding, X.; Wallace, G. G. Polypyrrole coated nylon lycra fabric as stretchable electrode for supercapacitor applications. *Electrochim. Acta* **2012**, *68*, 18–24.

[39] Jiang, H.; Sun, Y.; Rogers, J. A.; Huang, Y. Mechanics of precisely controlled thin film buckling on elastomeric substrate. *Appl. Phys. Lett.* **2007**, *90*, 133119.

[40] Chen, J.; Liu, H.; Weimer, W. A.; Halls, M. D.; Waldeck, D. H.; Walker, G. C. Noncovalent engineering of carbon nanotube surfaces by rigid, functional conjugated polymers. *J. Am. Chem. Soc.* **2002**, *124*, 9034–9035.

[41] Wu, T. M.; Lin, Y. W.; Liao, C. S. Preparation and characterization of polyaniline/multi-walled carbon nanotube composites. *Carbon* **2005**, *43*, 734–740.

[42] Yang, M.; Koutsos, V.; Zaiser, M. Interactions between polymers and carbon nanotubes: A molecular dynamics study. *J. Phys. Chem. B* **2005**, *109*, 10009–10014.

[43] Ma, W. J.; Song, L.; Yang, R.; Zhang, T. H.; Zhao, Y. C.; Sun, L. F.; Ren, Y.; Liu, D. F.; Liu, L. F.; Shen, J. et al. Directly synthesized strong, highly conducting, transparent single-walled carbon nanotube films. *Nano Lett.* **2007**, *7*, 2307–2311.

[44] Li, J.; Cassell, A.; Delzeit, L.; Han, J.; Meyyappan, M. Novel three-dimensional electrodes: Electrochemical properties of carbon nanotube ensembles. *J. Phys. Chem. B* **2002**, *106*, 9299–9305.

[45] Niu, Z. Q.; Ma, W. J.; Li, J. Z.; Dong, H. B.; Ren, Y.; Zhao, D.; Zhou, W. Y.; Xie, S. S. High-strength laminated copper matrix nanocomposites developed from a single-walled carbon nanotube film with continuous reticulate architecture. *Adv. Funct. Mater.* **2012**, *22*, 5209–5215.

[46] Niu, Z. Q.; Luan, P. S.; Shao, Q.; Dong, H. B.; Li, J. Z.; Chen, J.; Zhao, D.; Cai, L.; Zhou, W. Y.; Chen, X. D. et al. A "skeleton/skin" strategy for preparing ultrathin free-standing single-walled carbon nanotube/polyaniline films for high performance supercapacitor electrodes. *Energy Environ. Sci.* **2012**, *5*, 8726–8733.

[47] Ajayan, P. M.; Schadler, L. S.; Giannaris, C.; Rubio, A. Single-walled carbon nanotube–polymer composites: Strength and weakness. *Adv. Mater.* **2000**, *12*, 750–753.

[48] Hu, L. B.; Pasta, M.; La Mantia, F.; Cui, L. F.; Jeong, S.; Deshazer, H. D.; Choi, J. W.; Han, S. M.; Cui, Y. Stretchable, porous, and conductive energy textiles. *Nano Lett.* **2010**, *10*, 708–714.